

# Zwitterions in 3D Perovskites: Organosulfide-Halide Perovskites

Jiayi Li, Zhihengyu Chen, Santanu Saha, James K. Utterback, Michael L. Aubrey, Rongfeng Yuan, Hannah L. Weaver, Naomi S. Ginsberg, Karena W. Chapman, Marina R. Filip,\* and Hemamala I. Karunadasa\*



Cite This: <https://doi.org/10.1021/jacs.2c09382>



Read Online

ACCESS |



Metrics & More



Article Recommendations



Supporting Information

**ABSTRACT:** Although sulfide perovskites usually require high-temperature syntheses, we demonstrate that organosulfides can be used in the milder syntheses of halide perovskites. The zwitterionic organosulfide, cysteamine (CYS;  $^+\text{NH}_3(\text{CH}_2)_2\text{S}^-$ ), serves as both the  $\text{X}^-$  site and  $\text{A}^+$  site in the  $\text{ABX}_3$  halide perovskites, yielding the first examples of 3D organosulfide-halide perovskites:  $(\text{CYS})\text{PbX}_2$  ( $\text{X}^- = \text{Cl}^-$  or  $\text{Br}^-$ ). Notably, the band structures of  $(\text{CYS})\text{PbX}_2$  capture the direct bandgaps and dispersive bands of  $\text{APbX}_3$  perovskites. The sulfur orbitals compose the top of the valence band in  $(\text{CYS})\text{PbX}_2$ , affording unusually small direct bandgaps of 2.31 and 2.16 eV for  $\text{X}^- = \text{Cl}^-$  and  $\text{Br}^-$ , respectively, falling in the ideal range for the top absorber in a perovskite-based tandem solar cell. Measurements of the carrier dynamics in  $(\text{CYS})\text{PbCl}_2$  suggest carrier trapping due to defects or lattice distortions. The highly desirable bandgaps, band dispersion, and improved stability of the organosulfide perovskites demonstrated here motivate the continued expansion and exploration of this new family of materials, particularly with respect to extracting photocurrent. Our strategy of combining the  $\text{A}^+$  and  $\text{X}^-$  sites with zwitterions may offer more members in this family of mixed-anion 3D hybrid perovskites.

Halide perovskites have risen as contenders for low-cost and efficient solar-cell absorbers.<sup>1,2</sup> However, the composition that can deliver the desired efficiency and stability remains to be found.<sup>3</sup> In particular, a perovskite with a  $\sim 2$  eV bandgap is highly sought for the top absorber in a high-efficiency dual-<sup>4</sup> or triple-junction<sup>5</sup> tandem solar cell.<sup>6</sup> Although bromide-rich  $\text{A}^+\text{Pb}(\text{Br}_x\text{I}_{1-x})_3$  perovskites display such bandgaps, light-induced halide segregation precludes high voltages from being realized with these perovskites.<sup>7</sup> We therefore sought a different type of anion mixing to expand the accessible bandgaps of lead-halide perovskites. Herein, we report a new family of 3D halide perovskites, where a zwitterionic organosulfide serves as both the cationic A site and an anionic X site in the  $\text{A}^+\text{Pb}^{\text{II}}\text{X}_3$  ( $\text{X}^- = \text{halide}$ ) formula, yielding the general formula  $\text{LPb}^{\text{II}}\text{X}_2$  (here,  $\text{L} = \text{CYS} = ^+\text{NH}_3(\text{CH}_2)_2\text{S}^-$  and  $\text{X}^- = \text{Cl}^-$  or  $\text{Br}^-$ ). Notably, the calculated electronic structures of  $(\text{CYS})\text{PbX}_2$  show direct bandgaps and dispersive frontier bands—capturing the highly desirable characteristics of the  $\text{APbX}_3$  perovskites. Further, the dominant S contribution to the valence band reduces the bandgaps of  $(\text{CYS})\text{PbX}_2$  (2.31 and 2.16 eV for  $\text{X}^- = \text{Cl}^-$  and  $\text{Br}^-$ , respectively) compared to those of the  $(\text{MA})\text{PbX}_3$  perovskites (2.98 and 2.24 eV for  $\text{X}^- = \text{Cl}^-$  and  $\text{Br}^-$ , respectively). The substitution of heavier halides affords smaller bandgaps in perovskites, but at the cost of stability. In contrast, replacement of  $\text{Cl}^-$  or  $\text{Br}^-$  with  $\text{RS}^-$  reduces the perovskite's bandgap and enhances stability to moderate heat and high humidity.

Expanding the compositional diversity of halide perovskite solar absorbers is key for improving upon their drawbacks.<sup>8</sup> The direct bandgap of lead-halide perovskites is determined by the halide and lead frontier orbitals.<sup>9</sup> Thus, halide mixing is a common strategy for modulating the bandgap, explored since

the 1970s.<sup>10,11</sup> However, halide mobility<sup>12</sup> and light-induced halide segregation<sup>7</sup> impede stable optoelectronic properties from being realized in numerous mixed-halide compositions.

Anions such as  $\text{S}^{2-}$ ,  $\text{H}^-$ ,  $\text{N}^{3-}$ ,  $\text{Cl}^-$  have been substituted for the oxides in oxide perovskites.<sup>13–16</sup> In contrast, anion mixing in halide perovskites is limited to halides, and in 2D perovskites, to halides and pseudohalides ( $\text{SCN}^-$ ,  $\text{I}_3^-$ ).<sup>11</sup> Inspired by mixed-anion oxide perovskites, we sought to incorporate chalcogenides into halide perovskites. Sulfide perovskites such as  $\text{BaZrS}_3$  and  $\text{SrZrS}_3$  show bandgaps suitable for photovoltaic applications, and have greater heat and moisture stability compared to the halides.<sup>17</sup> However, sulfide perovskites are synthesized at high temperatures (800–1000 °C), and the study of their charge transport is in the early stages.<sup>18</sup> An obvious obstacle to introducing  $\text{S}^{2-}$  into halide perovskites is charge balance. We therefore considered organosulfides ( $\text{RS}^-$ ) as more suitable ligands to replace halides. To accommodate the larger organosulfides into a 3D perovskite, we combined the A site and the X site—essentially replacing  $\text{CH}_3\text{NH}_3^+$  and  $\text{X}^-$  with  $\text{R}^+\text{S}^-$  (Figure 1). We recently discovered that zwitterionic cysteamine (CYS) can template intergrowths in 2D perovskites to afford layered heterostructures.<sup>19</sup> The related disulfide ( $^+\text{H}_3\text{N}(\text{CH}_2)_2\text{S}-\text{S}(\text{CH}_2)_2\text{NH}_3^+$ )<sup>20</sup> and thiol ( $^+\text{H}_3\text{N}(\text{CH}_2)_2\text{SH}$ )<sup>21</sup> form 2D lead-

Received: September 2, 2022

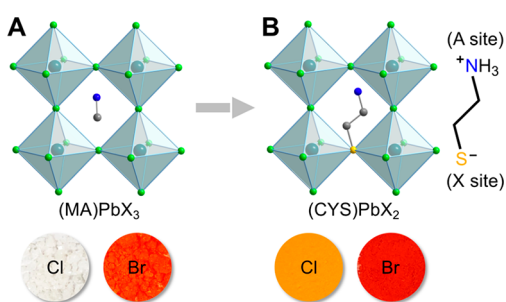


**Figure 1.** Conceptual derivation from (A)  $(MA)PbX_3$  ( $MA = CH_3NH_3^+$ ;  $X = \text{halide}$ ) to (B)  $(CYS)PbX_2$  ( $CYS = ^+NH_3(CH_2)_2S^-$ ) by combining the  $A^+$  site and  $X^-$  site into a zwitterion. Turquoise, green, yellow, blue, and gray spheres represent Pb, X, S, N, and C atoms, respectively. H atoms are not shown. Insets show the color of the perovskite powders.

halide perovskites. However, CYS has promising features for incorporation into a 3D perovskite: (1) the ammonium head in CYS may serve as the A site; (2) CYS is known to form Pb–S bonds;<sup>19,22,23</sup> and (3) the similarly sized ethylammonium has been incorporated into 3D perovskites, albeit in substoichiometric amounts.<sup>24</sup>

Combining equal amounts of  $PbX_2$  ( $X^- = Cl^-, Br^-$ ) and CYS in dimethylformamide at 150 °C under  $N_2$  affords a yellow or red solid, respectively, which was filtered while hot. Elemental analysis of the materials is consistent with the formula  $(CYS)PbX_2$ . Note that lower temperatures yield the perovskite heterostructure instead.<sup>19</sup> This method affords phase-pure  $(CYS)PbCl_2$ , although the synthesis of  $(CYS)PbBr_2$  contains ca. 5% of the heterostructure impurity. A mixture of CYS and CYS·HCl slows the crystallization to afford single crystals of  $(CYS)PbCl_2$  (Figure S1). Single-crystal X-ray diffraction revealed the structure as a 3D perovskite in the  $R\bar{3}c$  space group, with a heavily disordered organic component and indistinguishable Cl/S sites. Based on the formula, we expect each lead to be coordinated by 4 halides and 2 CYS molecules, on average. X-ray photoelectron spectroscopy (XPS) shows that the binding energies of S 2p in both  $(CYS)PbX_2$  and  $(Pb_2Cl_2)(CYS)_2PbCl_4$  are ca. 162 eV, within the typical energy range for metal sulfides (Figure S6),<sup>25</sup> whereas thiols (RSH) have a higher binding energy of 164 eV.<sup>26</sup> The  $^1H$  NMR spectra of the dissolved product confirmed that CYS is unchanged after forming the perovskites (Figure S7).

We then collected high-energy X-ray scattering data suitable for pair distribution function (PDF) and differential-envelope density (DED)<sup>27</sup> analyses using fine powders of  $(CYS)PbX_2$ . Since lighter elements have smaller X-ray scattering factors, the PDF signals mostly arise from the inorganic framework. The PDFs for both materials were modeled as 3D perovskites in the  $R\bar{3}c$  space group using the small-box structure model, considering only the inorganic framework (Figure 2A, 2B). Each anion site was modeled as 1/3 S and 2/3 X. We applied DED to compare the electron density of the preliminarily refined structure based on PDF with the experimental powder diffraction data. This analysis showed extra electron density in the cuboctahedral cavity of the perovskite (Figure S3), where we expect the cationic end of CYS to reside. The contribution from this disordered organic component ( $\sim C_2N = 19$  electrons) was modeled by a K atom (19 electrons) in the A site to improve the PDF fitting (Figure 2C). The experimental

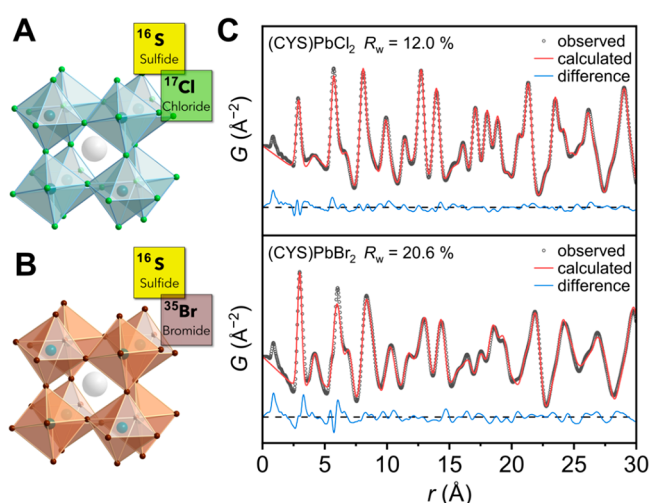


**Figure 2.** Room-temperature structures of (A)  $(CYS)PbCl_2$  and (B)  $(CYS)PbBr_2$  derived from pair distribution function (PDF) analysis with the disordered organoammonium tail of CYS represented by a gray sphere. Turquoise, green, brown, gray spheres represent Pb, Cl/S, Br/S, and K (proxy) atoms, respectively. (C) PDF analysis of  $(CYS)PbCl_2$  and  $(CYS)PbBr_2$ .

PXRD data and simulated patterns from the PDF models agree well (Figure S4).

We calculated the electronic band structures of  $(CYS)PbX_2$  within the generalized gradient approximation to density functional theory (DFT-PBE),<sup>28,29</sup> including spin–orbit coupling. We first built an ordered model for  $(CYS)PbX_2$  with a *trans* coordination of CYS to the Pb (Figure S8). The band structures of  $(CYS)PbX_2$  show direct gaps at  $\Gamma$  of 0.80 and 0.65 eV for  $X^- = Cl^-$  and  $Br^-$ , respectively (Figure 3A and 3B). The valence-band maximum (VBM) consists of 68% (60%) S and 29% (33%) Pb, with only 3% (7%) halogen for  $(CYS)PbCl_2$  ( $(CYS)PbBr_2$ ). In contrast, the VBM is 66% (57%) Pb and 34% (43%) halogen in  $CsPbCl_3$  ( $CsPbBr_3$ ) (Figure 3C and 3D). The conduction bands in both  $(CYS)PbX_2$  and  $CsPbX_3$  consist mostly of Pb contributions (Table S3). To test the sensitivity of our calculated band structures on the choice of S atom ordering, we then used  $Cs^+$  and  $HS^-$  as the  $A^+$  site and anion site, respectively (to mimic the zwitterionic CYS) and built hypothetical structures of  $Cs(HS)PbX_2$  in the rhombohedral supercell with (i) ordered *trans*  $HS^-$  and (ii) both *cis* and *trans* arrangements of  $HS^-$ . Comparison of the band structures for (i) and (ii) and for the ordered  $(CYS)PbX_2$  indicates that the band-edge dispersion is not especially sensitive to the arrangement of S atoms (Figure S10 and Table S4). To distinguish the impact of S on the electronic structure, without the accompanying structural changes, we then compared the band structure of  $(CYS)PbCl_2$  with that of a hypothetical  $CsPbCl_3$  with the Pb–Cl network fixed as in  $R\bar{3}c$   $(CYS)PbCl_2$  (Figure 4; Figure S11 for the bromide analogs). As expected, the band edges maintain a largely similar shape due to the isolobal frontier orbitals of  $RS^-$  and  $X^-$ . In addition, the presence of S reduces the bandgap by 0.7 eV. The anisotropy of the hole effective masses found for  $(CYS)PbX_2$  and  $Cs(HS)PbX_2$  is likely due to the presence and periodic ordering of S atoms in our computational models (Table S4).

Diffuse reflectance spectra of  $(CYS)PbX_2$  powders show strong absorption onsets, with optical gaps of 2.31 and 2.16 eV for  $(CYS)PbCl_2$  and  $(CYS)PbBr_2$  (Figure 5A), respectively,

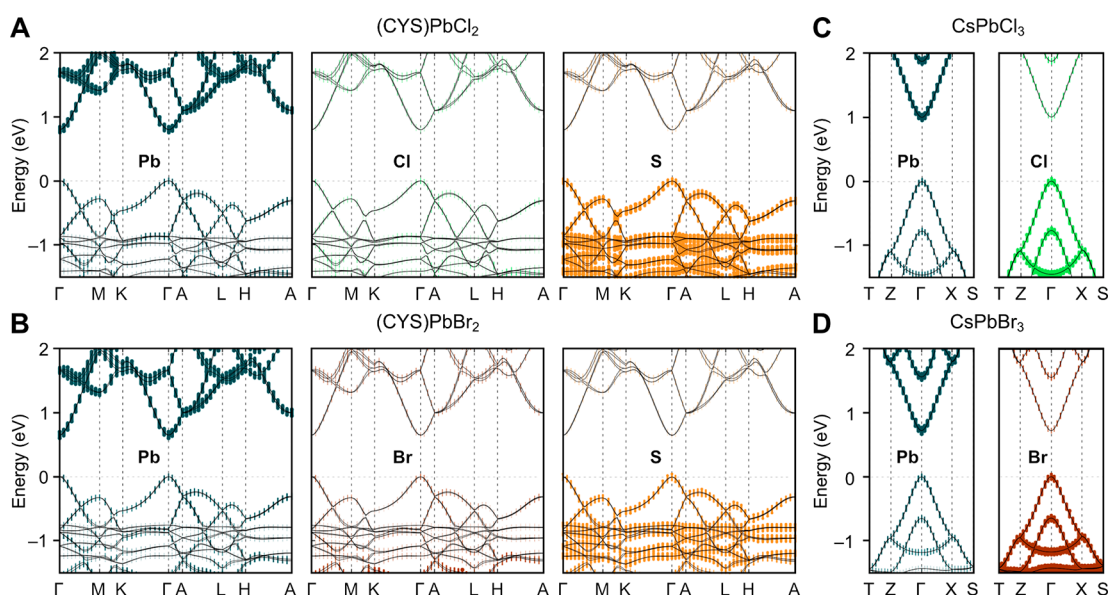


**Figure 3.** Band structures of (A) (CYS)PbCl<sub>2</sub>, (B) (CYS)PbBr<sub>2</sub>, (C) orthorhombic CsPbCl<sub>3</sub>, and (D) orthorhombic CsPbBr<sub>3</sub>. The Pb, Cl, Br, and S orbitals that contribute to the bands are represented by turquoise, green, brown, and orange dots, with the dot size proportional to the orbital contribution. The CYS molecules are modeled as ordered (see Supporting Information).

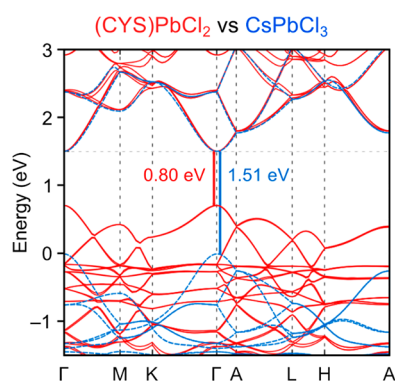


**Figure 4.** Comparison of the band structures of (CYS)PbCl<sub>2</sub> and hypothetical CsPbCl<sub>3</sub>, both in the *R3c* space group. The conduction band minima have been arbitrarily aligned.

calculated using direct-bandgap Tauc plots (Figure S12). The difference between the experimental bandgaps for (CYS)PbCl<sub>2</sub> and (CYS)PbBr<sub>2</sub> (0.15 eV) agrees with our DFT calculations

(0.15 eV). The bandgap of (CYS)PbCl<sub>2</sub> is smaller than that of orthorhombic (MA)PbCl<sub>3</sub> by ca. 0.7 eV, and the difference in bandgaps between chlorides and bromides is much smaller for (CYS)PbX<sub>2</sub> (0.15 eV) than for (MA)PbX<sub>3</sub> (0.74 eV). These features are consistent with the lesser electronegativity of S compared to Cl and the smaller halide contribution (<10%) in the VBM of (CYS)PbX<sub>2</sub>.

Although (MA)PbX<sub>3</sub> exhibits narrow, band-edge photoluminescence (PL) at room temperature (Figure S13), (CYS)PbX<sub>2</sub> shows broad PL only at low temperature (80 K; Figure 5A) with a large Stokes shift, suggesting strong electron–phonon interactions or the presence of defects. Similar broad PL from 2D Pb–X (X = Cl, Br) perovskites are attributed to exciton–phonon (self-trapping) interactions.<sup>30</sup> We further probed the carrier dynamics in (CYS)PbCl<sub>2</sub> single crystals. The weak room-temperature PL, measured by time-correlated single photon counting (TCSPC), exhibits an instrument response-limited component followed by a 0.9 ns decay (Figure 5B), which is similar to the PL lifetime of a (MA)PbCl<sub>3</sub> crystal (1.6 ns).<sup>31,32</sup> Some variation in the PL

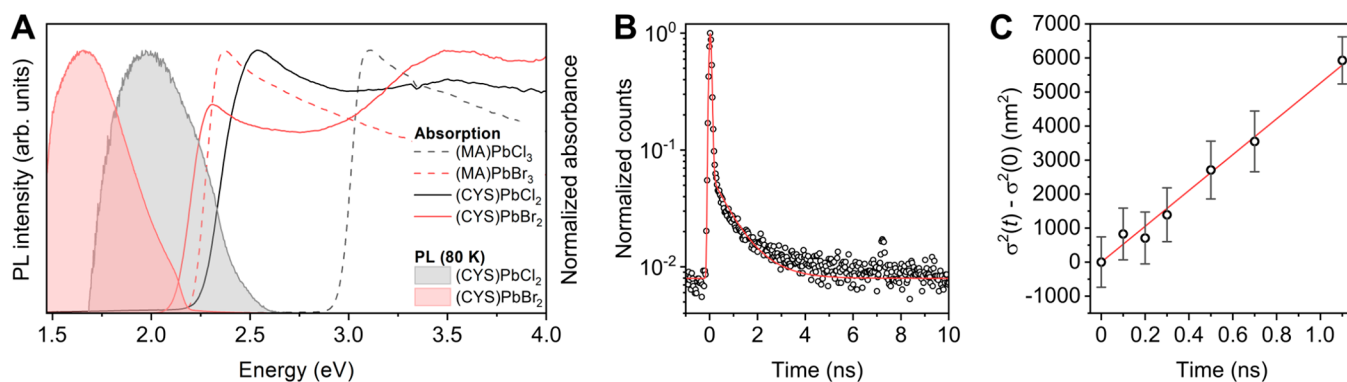


**Figure 5.** (A) Photoluminescence (PL) spectra of (CYS)PbX<sub>2</sub> (80 K, excitation: 340 nm) and diffuse reflectance spectra of (MA)PbX<sub>3</sub> (MA = CH<sub>3</sub>NH<sub>3</sub><sup>+</sup>; dotted lines) and (CYS)PbX<sub>2</sub> (solid lines). (B) Room-temperature PL decay trace of a (CYS)PbCl<sub>2</sub> crystal (excitation: 530 nm). (C) Mean-squared expansion curve fit from *t* = 100 ps to 1 ns (see text).

lifetime of different crystals (0.9–3.1 ns) is consistent with a defect-mediated emission.

We then applied stroboscopic scattering microscopy (stroboSCAT) to directly measure the microscopic carrier behavior.<sup>33–35</sup> We excited a (CYS)PbCl<sub>2</sub> crystal with a 470 nm light pulse (~100 ps pulse) focused to a 278 nm spot size (full width at half maximum). The resulting excited carrier profile was imaged using a time-delayed widefield 635 nm probe light pulse. The image contrast is proportional to the carrier-induced changes to the material's refractive index.<sup>33,34</sup> Comparing images at different pump–probe time delays to dark reference images gives the spatiotemporal transient reflectance images,  $\Delta R/R$  (Figure S14). We fit the radial expansion of the carrier distribution to a Gaussian profile of width  $\sigma$  over time  $t$  to find the mean-squared expansion,  $\sigma^2(t) - \sigma^2(0)$ . The mean-squared expansion is nonlinear, transitioning from a relatively high diffusivity ( $D_{\text{fast}}$ ), which persists over 100 ps–1 ns, to a lower diffusivity ( $D_{\text{slow}}$ ) that persists to at least 100 ns (Figure S15). Fitting the mean-squared expansion to  $2Dt$  for  $t = 100$  ps to 1 ns (Figure 5C), where carriers persist in the emissive state measured by TCSPC, gives  $D_{\text{fast}} = 3.1(2) \times 10^{-2}$  cm<sup>2</sup>/s. This value can be related to the mobility ( $\mu$ ) through the Einstein relation,  $eD = \mu k_{\text{B}}T$ —where  $e$  is the elementary charge,  $k_{\text{B}}$  is the Boltzmann constant, and  $T$  is the temperature—to give  $\mu = 1.4$  cm<sup>2</sup>/V·s. The lower mobility in (CYS)PbCl<sub>2</sub> compared to that of a (MA)PbCl<sub>3</sub> single crystal (42 cm<sup>2</sup>/V·s)<sup>36</sup> could be due to surface defects or enhanced carrier/exciton–phonon coupling in (CYS)PbCl<sub>2</sub>, as seen in other chloride perovskites.<sup>37,38</sup>

The (CYS)PbX<sub>2</sub> perovskites exhibit higher stability toward moisture and extended mild heating compared to (MA)PbX<sub>3</sub>, which may be due to the Pb–S covalency. The PXRD patterns of (CYS)PbX<sub>2</sub> after moisture exposure (100% RH, 10 days for X<sup>−</sup> = Cl<sup>−</sup> and 5 days for X<sup>−</sup> = Br<sup>−</sup>) or heating (60 °C in air, 30 days for X<sup>−</sup> = Cl<sup>−</sup> and 15 days for X<sup>−</sup> = Br<sup>−</sup>) showed no evidence of decomposition (Figure S18). In contrast, (MA)PbX<sub>3</sub> showed decomposition after exposure to the 100% RH (1 day for X<sup>−</sup> = Cl<sup>−</sup> and Br<sup>−</sup>) or heating at 60 °C (10 days for X<sup>−</sup> = Cl<sup>−</sup> and 8 days for X<sup>−</sup> = Br<sup>−</sup>). Thermal stability at higher temperatures is discussed in the Supporting Information.

Organosulfides allow sulfur to be incorporated into lead-halide perovskites at mild temperatures, circumventing the formation of PbS. The new LPbX<sub>2</sub> perovskites (L = zwitterion) largely preserve the desirable electronic band structure of the APbX<sub>3</sub> perovskites. Incorporating heavier halides and chalcogenides into LPbX<sub>2</sub> and passivating defects may improve carrier mobility for charge extraction. Overall, (CYS)PbX<sub>2</sub> combines characteristics of PbS and APbX<sub>3</sub>—two important families of solar absorbers—and we expect that these are the first members of a larger family of organochalcogenide-halide perovskites.

## ■ ASSOCIATED CONTENT

### Supporting Information

The Supporting Information is available free of charge at <https://pubs.acs.org/doi/10.1021/jacs.2c09382>.

Experimental and computational details, crystallographic data, and spectra (PDF)

### Accession Codes

CCDC 2205034 contains the supplementary crystallographic data for this paper. These data can be obtained free of charge via [www.ccdc.cam.ac.uk/data\\_request/cif](http://www.ccdc.cam.ac.uk/data_request/cif), or by emailing

[data\\_request@ccdc.cam.ac.uk](mailto:data_request@ccdc.cam.ac.uk), or by contacting The Cambridge Crystallographic Data Centre, 12 Union Road, Cambridge CB2 1EZ, UK; fax: +44 1223 336033.

## ■ AUTHOR INFORMATION

### Corresponding Authors

**Marina R. Filip** – Department of Physics, University of Oxford, Oxford OX1 3PU, United Kingdom; [orcid.org/0000-0003-2925-172X](https://orcid.org/0000-0003-2925-172X); Email: [marina.filip@physics.ox.ac.uk](mailto:marina.filip@physics.ox.ac.uk)

**Hemamala I. Karunadasa** – Department of Chemistry, Stanford University, Stanford, California 94305, United States; Stanford Institute for Materials and Energy Sciences, SLAC National Accelerator Laboratory, Menlo Park, California 94025, United States; [orcid.org/0000-0003-4949-8068](https://orcid.org/0000-0003-4949-8068); Email: [hemamala@stanford.edu](mailto:hemamala@stanford.edu)

### Authors

**Jiayi Li** – Department of Chemistry, Stanford University, Stanford, California 94305, United States

**Zhihengyu Chen** – Department of Chemistry, Stony Brook University, Stony Brook, New York 11794, United States; [orcid.org/0000-0001-5882-7076](https://orcid.org/0000-0001-5882-7076)

**Santanu Saha** – Department of Physics, University of Oxford, Oxford OX1 3PU, United Kingdom

**James K. Utterback** – Department of Chemistry, University of California, Berkeley, California 94720, United States; [orcid.org/0000-0002-2926-841X](https://orcid.org/0000-0002-2926-841X)

**Michael L. Aubrey** – Department of Chemistry, Stanford University, Stanford, California 94305, United States; Present Address: M.L.A.: Department of Chemistry, University of Texas at Austin, Texas, 78712, United States; [orcid.org/0000-0002-0740-0731](https://orcid.org/0000-0002-0740-0731)

**Rongfeng Yuan** – Department of Chemistry, University of California, Berkeley, California 94720, United States; [orcid.org/0000-0002-6572-2472](https://orcid.org/0000-0002-6572-2472)

**Hannah L. Weaver** – Department of Chemistry, University of California, Berkeley, California 94720, United States

**Naomi S. Ginsberg** – Department of Chemistry, University of California, Berkeley, California 94720, United States; STROBE, National Science Foundation Science and Technology Center and Department of Physics, University of California Berkeley, Berkeley, California 94720, United States; Materials Science Division and Molecular Biophysics and Integrated Bioimaging Division, Lawrence Berkeley National Laboratory, Berkeley, California 94720, United States; Kavli Energy NanoSciences Institute at Berkeley, Berkeley, California 94720, United States; [orcid.org/0000-0002-5660-3586](https://orcid.org/0000-0002-5660-3586)

**Karena W. Chapman** – Department of Chemistry, Stony Brook University, Stony Brook, New York 11794, United States; [orcid.org/0000-0002-8725-5633](https://orcid.org/0000-0002-8725-5633)

Complete contact information is available at: <https://pubs.acs.org/doi/10.1021/jacs.2c09382>

### Notes

The authors declare no competing financial interest.

## ■ ACKNOWLEDGMENTS

This work was supported by the Brown Science Foundation. J.L. acknowledges a Stanford Interdisciplinary Graduate Fellowship and M.L.A. acknowledges an Office of Energy Efficiency and Renewable Energy (EERE) postdoctoral

fellowship. M.R.F. acknowledges support of the John Fell Oxford University Press (OUP) Research Fund. S.S. and M.R.F. acknowledge support from the UK Engineering and Physical Sciences Research Council (EPSRC), Grant EP/V010840/1. S.S. and M.R.F. accessed computational resources accessed via our membership of the UK's HEC Materials Chemistry Consortium, which is funded by EPSRC (EP/R029431). SCXRD studies were performed at the Stanford Nano Shared Facilities (SNSF), supported by the National Science Foundation (NSF) under award ECCS-1542152. This research used resources of the Advanced Photon Source, a U.S. Department of Energy (DOE) Office of Science User Facility operated for the DOE Office of Science by Argonne National Laboratory under contract no. DE-AC02-06CH11357. The stroboSCAT measurements and analysis were supported by STROBE, a NSF Science & Technology Center under Grant No. DMR 1548924. J.K.U. acknowledges support from the Arnold O. Beckman Postdoctoral Fellowship in the Chemical Sciences. R.Y. acknowledges support from the Camille and Henry Dreyfus Foundation's Postdoctoral Program in Environmental Chemistry. N.S.G. acknowledges a David and Lucile Packard Foundation Fellowship for Science and Engineering and a Camille and Henry Dreyfus Teacher-Scholar Award.

## REFERENCES

- (1) Kojima, A.; Teshima, K.; Shirai, Y.; Miyasaka, T. Organometal Halide Perovskites as Visible-Light Sensitizers for Photovoltaic Cells. *J. Am. Chem. Soc.* **2009**, *131* (17), 6050–6051.
- (2) Green, M. A.; Ho-Baillie, A.; Snaith, H. J. The Emergence of Perovskite Solar Cells. *Nat. Photonics* **2014**, *8* (7), 506–514.
- (3) Rong, Y.; Hu, Y.; Mei, A.; Tan, H.; Saidaminov, M. I.; Seok, S. I.; McGehee, M. D.; Sargent, E. H.; Han, H. Challenges for Commercializing Perovskite Solar Cells. *Science* **2018**, *361* (6408), eaat8235.
- (4) Crisp, R. W.; Pach, G. F.; Kurley, J. M.; France, R. M.; Reese, M. O.; Nanayakkara, S. U.; MacLeod, B. A.; Talapin, D. V.; Beard, M. C.; Luther, J. M. Tandem Solar Cells from Solution-Processed CdTe and PbS Quantum Dots Using a ZnTe–ZnO Tunnel Junction. *Nano Lett.* **2017**, *17* (2), 1020–1027.
- (5) Derendorf, K.; Essig, S.; Oliva, E.; Klinger, V.; Roesener, T.; Philipps, S. P.; Benick, J.; Hermle, M.; Schachtner, M.; Siefer, G.; Jäger, W.; Dimroth, F. Fabrication of GaInP/GaAs//Si Solar Cells by Surface Activated Direct Wafer Bonding. *IEEE J. Photovolt.* **2013**, *3* (4), 1423–1428.
- (6) Wang, R.; Huang, T.; Xue, J.; Tong, J.; Zhu, K.; Yang, Y. Prospects for Metal Halide Perovskite-Based Tandem Solar Cells. *Nat. Photonics* **2021**, *15* (6), 411–425.
- (7) Hoke, E. T.; Slotcavage, D. J.; Dohner, E. R.; Bowering, A. R.; Karunadasa, H. I.; McGehee, M. D. Reversible Photo-Induced Trap Formation in Mixed-Halide Hybrid Perovskites for Photovoltaics. *Chem. Sci.* **2015**, *6* (1), 613–617.
- (8) Slavney, A. H.; Smaha, R. W.; Smith, I. C.; Jaffe, A.; Umeyama, D.; Karunadasa, H. I. Chemical Approaches to Addressing the Instability and Toxicity of Lead–Halide Perovskite Absorbers. *Inorg. Chem.* **2017**, *56* (1), 46–55.
- (9) Umebayashi, T.; Asai, K.; Kondo, T.; Nakao, A. Electronic Structures of Lead Iodide Based Low-Dimensional Crystals. *Phys. Rev. B* **2003**, *67* (15), 155405.
- (10) Donaldson, J. D.; Laughlin, D.; Ross, S. D.; Silver, J. Phases Obtained from the Frozen Molten Systems Caesium–Tin–Halide and Caesium–Lead–Halide. *J. Chem. Soc., Dalton Trans.* **1973**, *19*, 1985–1988.
- (11) Matheu, R.; Vigil, J. A.; Crace, E. J.; Karunadasa, H. I. The Halogen Chemistry of Halide Perovskites. *Trends Chem.* **2022**, *4* (3), 206–219.
- (12) Kim, G. Y.; Senocrate, A.; Wang, Y.-R.; Moia, D.; Maier, J. Photo-Effect on Ion Transport in Mixed Cation and Halide Perovskites and Implications for Photo-Demixing\*\*. *Angew. Chem., Int. Ed.* **2021**, *60* (2), 820–826.
- (13) Harada, J. K.; Charles, N.; Poeppelmeier, K. R.; Rondinelli, J. M. Heteroanionic Materials by Design: Progress Toward Targeted Properties. *Adv. Mater.* **2019**, *31* (19), 1805295.
- (14) Kobayashi, Y.; Tsujimoto, Y.; Kageyama, H. Property Engineering in Perovskites via Modification of Anion Chemistry. *Annu. Rev. Mater. Res.* **2018**, *48* (1), 303–326.
- (15) Kageyama, H.; Hayashi, K.; Maeda, K.; Atfield, J. P.; Hiroi, Z.; Rondinelli, J. M.; Poeppelmeier, K. R. Expanding Frontiers in Materials Chemistry and Physics with Multiple Anions. *Nat. Commun.* **2018**, *9* (1), 772.
- (16) Ran, J.; Wang, T.; Zhang, J.; Liu, Y.; Xu, C.; Xi, S.; Gao, D. Modulation of Electronics of Oxide Perovskites by Sulfur Doping for Electrocatalysis in Rechargeable Zn–Air Batteries. *Chem. Mater.* **2020**, *32* (8), 3439–3446.
- (17) Swarnkar, A.; Mir, W. J.; Chakraborty, R.; Jagadeeswararao, M.; Sheikh, T.; Nag, A. Are Chalcogenide Perovskites an Emerging Class of Semiconductors for Optoelectronic Properties and Solar Cell? *Chem. Mater.* **2019**, *31* (3), 565–575.
- (18) Suhail, M.; Abbas, H.; Khan, M. B.; Khan, Z. H. Chalcogenide Perovskites for Photovoltaic Applications: A Review. *J. Nanoparticle Res.* **2022**, *24* (7), 142.
- (19) Aubrey, M. L.; Saldivar Valdes, A.; Filip, M. R.; Connor, B. A.; Lindquist, K. P.; Neaton, J. B.; Karunadasa, H. I. Directed Assembly of Layered Perovskite Heterostructures as Single Crystals. *Nature* **2021**, *597* (7876), 355–359.
- (20) Lemmerer, A.; Billing, D. G. Effect of Heteroatoms in the Inorganic–Organic Layered Perovskite-Type Hybrids [(ZC<sub>n</sub>H<sub>2n</sub>NH<sub>3</sub>)<sub>2</sub>PbI<sub>4</sub>], n = 2, 3, 4, 5, 6; Z = OH, Br and I; and [(H<sub>3</sub>NC<sub>2</sub>H<sub>4</sub>S<sub>2</sub>C<sub>2</sub>H<sub>4</sub>NH<sub>3</sub>)PbI<sub>4</sub>]. *CrystEngComm* **2010**, *12* (4), 1290–1301.
- (21) Kour, P.; Chenna Reddy, M.; Pal, S.; Sidhik, S.; Das, T.; Pandey, P.; Mukherjee, S. P.; Chakraborty, S.; Mohite, A. D.; Ogale, S. An Organic–Inorganic Perovskitoid with Zwitterion Cysteamine Linker and Its Crystal–Crystal Transformation to Ruddlesden–Popper Phase. *Angew. Chem., Int. Ed.* **2021**, *60* (34), 18750–18760.
- (22) Fleischer, H.; Schollmeyer, D. Synthesis of and Structural Studies on Lead(II) Cysteamin Complexes. *Inorg. Chem.* **2004**, *43* (18), 5529–5536.
- (23) Bharara, M. S.; Parkin, S.; Atwood, D. A. Two-Dimensional Network Acquired by Pb(II)–2-Aminoethanethiolate. *Inorg. Chim. Acta* **2006**, *359* (10), 3375–3378.
- (24) Peng, W.; Miao, X.; Adinolfi, V.; Alarousu, E.; El Tall, O.; Emwas, A.-H.; Zhao, C.; Walters, G.; Liu, J.; Ouellette, O.; Pan, J.; Murali, B.; Sargent, E. H.; Mohammed, O. F.; Bakr, O. M. Engineering of CH<sub>3</sub>NH<sub>3</sub>PbI<sub>3</sub> Perovskite Crystals by Alloying Large Organic Cations for Enhanced Thermal Stability and Transport Properties. *Angew. Chem., Int. Ed.* **2016**, *55* (36), 10686–10690.
- (25) Moulder, J. F. *Handbook of X-Ray Photoelectron Spectroscopy*.
- (26) Castner, D. G.; Hinds, K.; Grainger, D. W. X-Ray Photoelectron Spectroscopy Sulfur 2p Study of Organic Thiol and Disulfide Binding Interactions with Gold Surfaces. *Langmuir* **1996**, *12* (21), 5083–5086.
- (27) Yakovenko, A. A.; Wei, Z.; Wriedt, M.; Li, J.-R.; Halder, G. J.; Zhou, H.-C. Study of Guest Molecules in Metal–Organic Frameworks by Powder X-Ray Diffraction: Analysis of Difference Envelope Density. *Cryst. Growth Des.* **2014**, *14* (11), 5397–5407.
- (28) Hohenberg, P.; Kohn, W. Inhomogeneous Electron Gas. *Phys. Rev.* **1964**, *136* (3B), B864–B871.
- (29) Perdew, J. P.; Burke, K.; Ernzerhof, M. Generalized Gradient Approximation Made Simple. *Phys. Rev. Lett.* **1996**, *77* (18), 3865–3868.
- (30) Dohner, E. R.; Jaffe, A.; Bradshaw, L. R.; Karunadasa, H. I. Intrinsic White-Light Emission from Layered Hybrid Perovskites. *J. Am. Chem. Soc.* **2014**, *136* (38), 13154–13157.

(31) Jung, H. R.; Cho, Y.; Jo, W. UV and Visible Photodetectors of MAPbBr<sub>3</sub> and MAPbCl<sub>3</sub> Perovskite Single Crystals via Single Photocarrier Transport Design. *Adv. Opt. Mater.* **2022**, *10* (7), 2102175.

(32) Yuan, Z.; Huang, W.; Ma, S.; Ouyang, G.; Hu, W.; Zhang, W. A High Performance Perovskite CH<sub>3</sub>NH<sub>3</sub>PbCl<sub>3</sub> Single Crystal Photodetector: Benefiting from an Evolutionary Preparation Process. *J. Mater. Chem. C* **2019**, *7* (18), 5442–5450.

(33) Delor, M.; Weaver, H. L.; Yu, Q.; Ginsberg, N. S. Imaging Material Functionality through Three-Dimensional Nanoscale Tracking of Energy Flow. *Nat. Mater.* **2020**, *19* (1), 56–62.

(34) Delor, M.; Slavney, A. H.; Wolf, N. R.; Filip, M. R.; Neaton, J. B.; Karunadasa, H. I.; Ginsberg, N. S. Carrier Diffusion Lengths Exceeding 1 Mm Despite Trap-Limited Transport in Halide Double Perovskites. *ACS Energy Lett.* **2020**, *5* (5), 1337–1345.

(35) Folie, B. D.; Tan, J. A.; Huang, J.; Sercel, P. C.; Delor, M.; Lai, M.; Lyons, J. L.; Bernstein, N.; Efros, A. L.; Yang, P.; Ginsberg, N. S. Effect of Anisotropic Confinement on Electronic Structure and Dynamics of Band Edge Excitons in Inorganic Perovskite Nanowires. *J. Phys. Chem. A* **2020**, *124* (9), 1867–1876.

(36) Herz, L. M. Charge-Carrier Mobilities in Metal Halide Perovskites: Fundamental Mechanisms and Limits. *ACS Energy Lett.* **2017**, *2* (7), 1539–1548.

(37) Luo, J.; Wang, X.; Li, S.; Liu, J.; Guo, Y.; Niu, G.; Yao, L.; Fu, Y.; Gao, L.; Dong, Q.; Zhao, C.; Leng, M.; Ma, F.; Liang, W.; Wang, L.; Jin, S.; Han, J.; Zhang, L.; Etheridge, J.; Wang, J.; Yan, Y.; Sargent, E. H.; Tang, J. Efficient and Stable Emission of Warm-White Light from Lead-Free Halide Double Perovskites. *Nature* **2018**, *563* (7732), 541–545.

(38) Crace, E.; Su, A.; Karunadasa, H. I. Reliably Obtaining White Light from Layered Halide Perovskites at Room Temperature. *Chem. Sci.* **2022**, *13*, 9973.